AD-A173 936 DYNAMIC BEHAVIOR OF REACTING GAS JETS SUBMERGED IN LIQUIDS: A PHOTOGRAPHIC STUDY(U) ARGONNE NATIONAL LAB IL D H CHO ET AL SEP 86 ANL-86-41 N00014-85-F-0086 1/1

UNCLASSIFIED F/G 21/2 NL

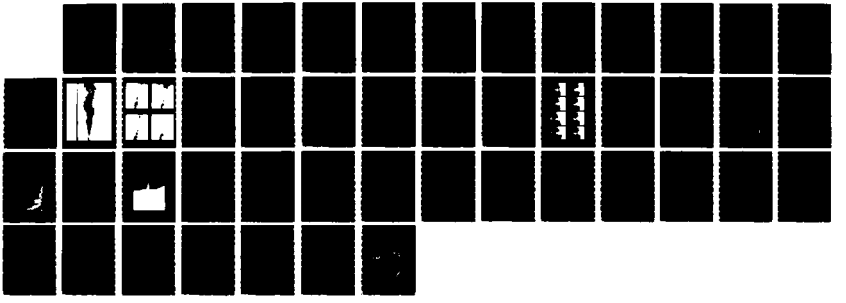

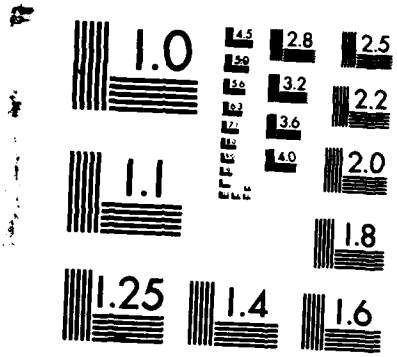

ANL-86-41

(12)

Reactor Analysis and Safety Division
Reactor Analysis and Safety Division
Reactor Analysis and Safety Division

Dynamic Behavior of Reacting Gas Jets Submerged in Liquids: A Photographic Study

by D. H. Cho, D. R. Armstrong, and L. Bova

Argonne National Laboratory, Argonne, Illinois 60439
operated by The University of Chicago
Prepared for the Department of the Navy
Office of Naval Research, Arlington, VA 22217

Printed in the United States of America
Available from
National Technical Information Service
U. S. Department of Commerce
5285 Port Royal Road
Springfield, VA 22161

NTIS price codes
Printed copy: A03
Microfiche copy: A01

ANL-86-41

ARGONNE NATIONAL LABORATORY
9700 South Cass Avenue
Argonne, Illinois 60439

DYNAMIC BEHAVIOR OF REACTING GAS JETS SUBMERGED IN LIQUIDS: A PHOTOGRAPHIC STUDY

Annual Report
For the Period May 1, 1985 to May 1, 1986

D. H. Cho, D. R. Armstrong and L. Bova

Reactor Analysis and Safety Division

September 1986

Prepared for the Department of the Navy
Office of Naval Research
Arlington, VA 22217

Under Contract No. N00014-85-F-0086

TABLE OF CONTENTS

LIST OF FIGURES

NOMENCLATURE

C_p	Specific heat of bath liquid
C_1, C_2, C_3 C_4	Constants
d_o	Injector nozzle diameter
ΔH_{rea}	Heat of reaction
ΔH_{vap}	Latent heat of vaporization
L	Plume length
L_c	Condensation length
L_d	Dissolution length
L_r	Reaction length
$\dot{m}_o$	Oxidizer gas flow rate or injector nozzle
$\dot{m}_\infty$	Entrainment rate of bath liquid into gas jet
P_s	Oxidizer gas plenum stagnation pressure
T_{sat}	Boiling point of bath liquid
T_∞	Temperature of bath liquid
ΔT	$T_{sat} - T_\infty$
X_{vap}	Vapor quality
$Y_{F\infty}$	Mass fraction of fuel in bath liquid
Y^*_{HCl}	HCl gas mass fraction corresponding to solubility limit in water
ϕ	Stoichiometric fuel-to-oxidizer mass ratio
ρ_o	Density of oxygen gas at nozzle exit
ρ_∞	Density of bath liquid

Abstract

A photographic study of a hydrogen chloride gas jet reacting in an aqueous solution of ammonia was conducted. The high-speed motion pictures taken revealed that the behavior of the reacting gas jet was highly dynamic and complex. The gaseous jet penetration ("plume") was not stationary, but underwent a change in shape and size with time, which appeared to be periodic or cyclic. Certain observations made, including a high-pitched sound, exhibited a striking similarity to the so-called "singing flame" phenomenon. Such dynamic plume behavior is attributed to the vaporization of the bath liquid due to reaction heat release. The plume length measurements for large concentrations of ammonia seem to confirm the prediction that when the extent of vaporization is large, the plume length is mainly determined by the distance required for condensation of the vapor.

I. Introduction

Power systems based on liquid metal combustion are attractive for underwater applications due to the relatively high heat of reaction and the absence of gaseous combustion products. While the feasibility of a metal-combustion power system has been demonstrated in laboratory tests, the parameters and mechanisms controlling the combustion reaction are not adequately understood. It would be expected that the chemical kinetics of metal combustion reactions is so fast that the reactions are usually controlled by mixing and transport processes. It appears, however, that little work has been done on the detailed mechanisms of these controlling processes, except for the pioneering studies by Faeth and his co-workers [5,6].

Recently, an experimental program has been initiated at Argonne National Laboratory to investigate in detail the reaction zone structure of an oxidizer gas jet submerged in a liquid metal fuel. In this investigation, a single, sonic jet of chlorine gas will be injected into molten baths of pure sodium with the objective of characterizing the reaction zone and its immediate environment. Flash X-ray pictures will be taken of the reacting gaseous jet. A fiber optic pyrometer will be employed to measure the reaction zone temperature. Temperature gradients in the near environment of the reaction zone will be measured using thermocouple arrays.

As a prelude to the sodium/chlorine experiment, a series of photographic experiments using a simulant pair of reactants have been conducted. In these experiments, pure hydrogen chloride (HCl) gas was injected into an aqueous solution of ammonia (NH_3). There were two reasons for choosing the NH_3/HCl system. First, it would provide new data for chemically reacting gas jets, especially for situations where the reaction zone length is expected to be short. Second and perhaps more important, an examination of the energetics of

the NH_3/HCl and Na/Cl_2 systems vis-a-vis the latent heat of fuel vaporization suggested that these two systems would have similar potential for fuel vaporization due to the heat of reaction. The fuel vaporization would have an important effect on the reaction zone structure, since it would influence the reaction mechanism (e.g. gas/liquid interface vs. gas-phase reaction) as well as the mi ng of the gaseous oxidizer jet and liquid fuel. This report summarizes the results of the NH_3/HCl experiments, which seem to indicate the importance of fuel vaporization in understanding the behavior of a reacting gaseous jet in liquids.

II. Apparatus and Procedure

As shown in Fig. 1, the apparatus for the simulant materials experiments centers on a reaction vessel made of a vertical 45 cm section of 10 cm ID glass pipe. The bottom of the vessel is a flat stainless steel plate with a center hole and fitting to accommodate a 1/4" OD tube and nozzle, a flush mounted pressure transducer, an electrical heater and a drain valve. The top is another flat plate with a thermocouple feedthrough and three valved holes (the heater, thermocouple and some of the valves are not shown in Fig. 1). One of the holes serves as an inlet for filling the vessel with the liquid reactant while the other two are exhausts. One goes directly to the building ventilation and the other goes through a packed bed scrubber filled with a solution of sodium dihydrogen phosphate that will neutralize any HCl or NH_3 gas from the reaction vessel.

The nozzle, as shown in Fig. 2, is inserted 5 cm from the bottom of the vessel. It is connected through a three-way ball valve to an argon purge line and the hydrogen chloride supply line. A pressure gauge in the line measures the upstream pressure of the semiconductor grade HCl supplied from a commercial cylinder through a pressure regulator.

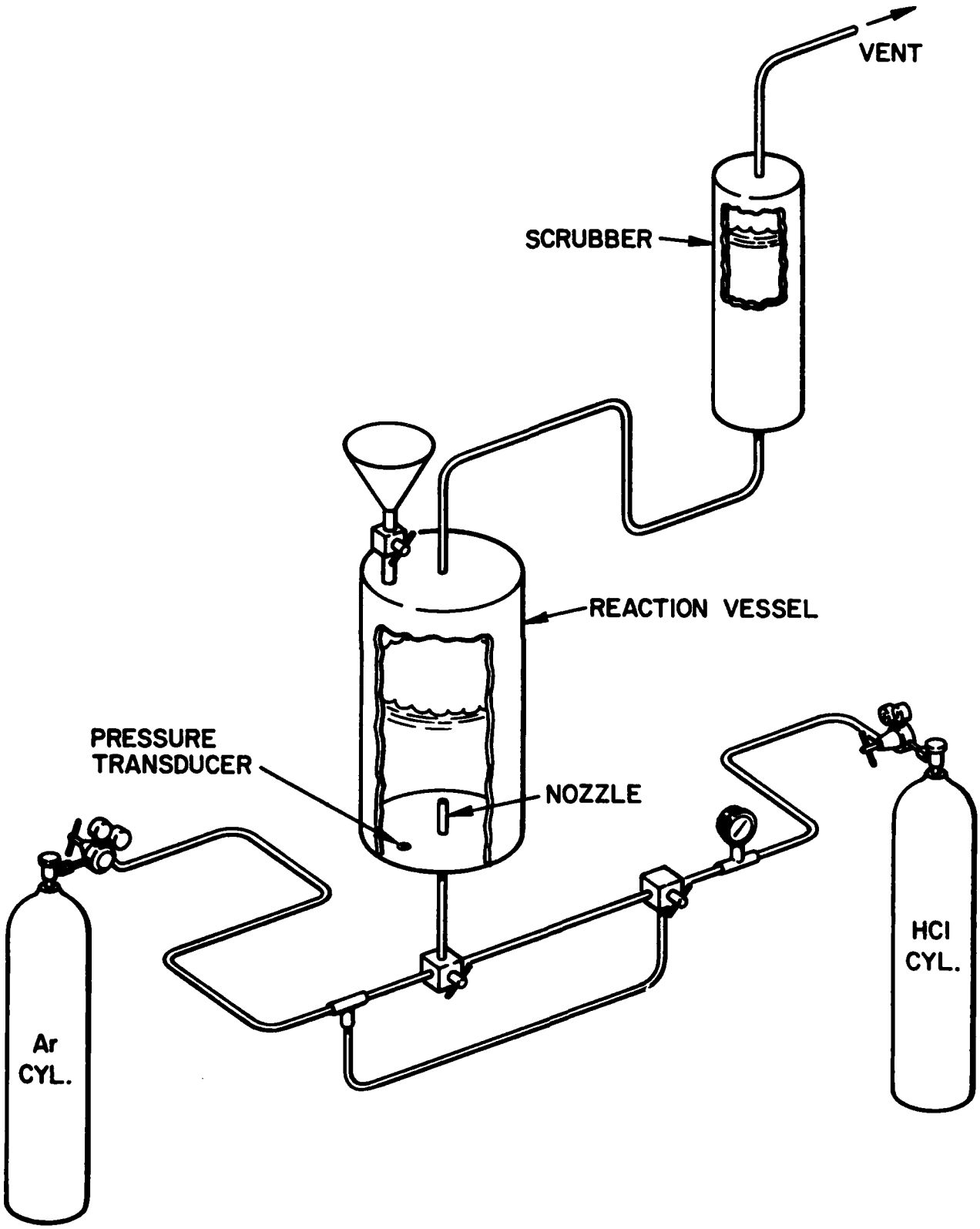

Fig. 1. Experimental Apparatus

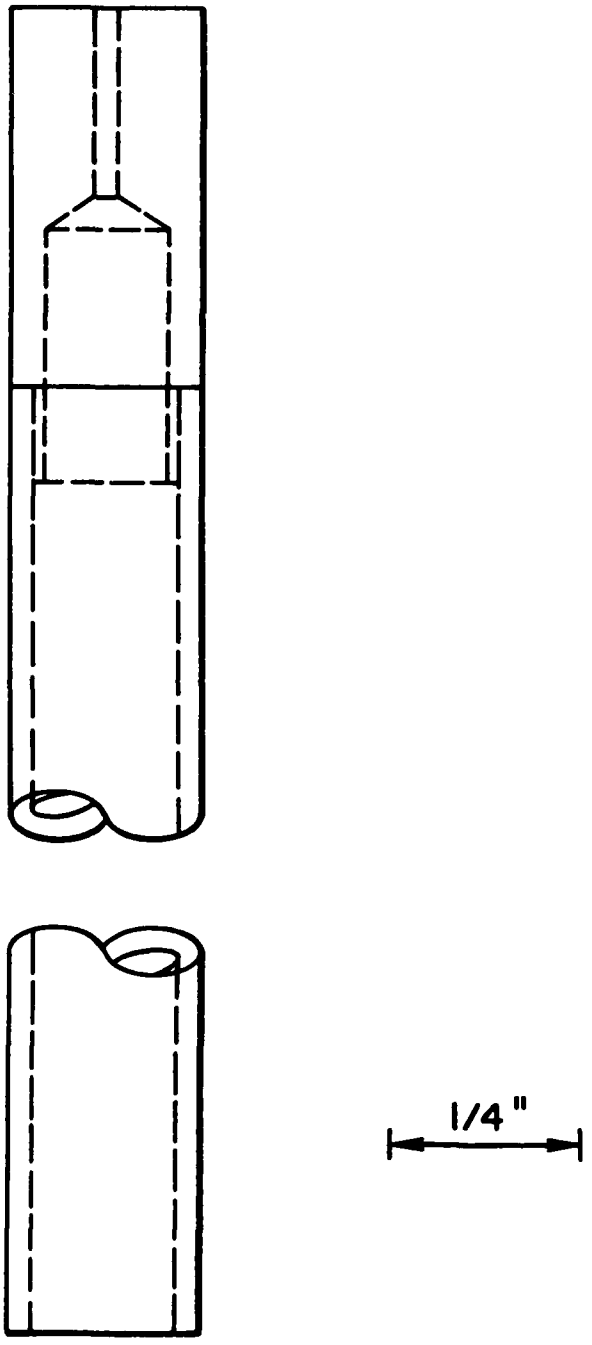

Fig. 2. Injector Nozzle

The flush mounted pressure transducer at the bottom of the reaction vessel is of a piezoelectric type and measures pressure fluctuations in the ammonia solution. It is located at a distance of 3.8 cm from the nozzle tube axis (6.3 cm from the nozzle exit).

Either high speed movies or single frames using a 200 μsec strobo light can be taken of the jet behavior. Signals from the pressure transducer can be displayed on an oscilloscope or superimposed on the motion pictures.

The operating procedure for a normal experiment began with the installation of the selected nozzle. The reaction vessel was then filled with two liters of pre-mixed aqueous solution of ammonia. Argon was run through the nozzle for several seconds to check the operation of the system. A sample of the solution was drawn off through the drain valve and saved for later chemical analysis. The HCl supply to the nozzle was then valved on and photographic and pressure records were taken. The nozzle was switched from HCl to argon after about 10 seconds of operation. (After ten seconds a myriad of small bubbles appeared, obscuring the view of the jet and thus making it virtually impossible to take a good photograph. It is presumed that the bubbles were of non-reacting gas contaminants of the HCl stream.) The argon purge was continued for about ten seconds to clean the nozzle of HCl and reduce corrosion of the equipment. The HCl injection was repeated as necessary. A final sample of the solution was taken. Then the vessel was drained and the nozzle and pressure transducer were removed and cleaned. The initial and final solution samples were titrated with a standard solution of HCl to determine the concentration of NH_4OH.

III. Plume Lengths

Prior to making runs with reacting jets, a series of preliminary experiments were conducted using an air jet submerged in water. The purpose of these experiments was to evaluate the design of gas injection nozzles. Various designs of 1-mm diameter straight-bore nozzles were tested and no significant differences in the hydrodynamic behavior of gas jets were noticed. For all tests the plenum pressure was sufficiently great that the flow was always choked at the nozzle. An interesting observation common to the various designs was the occurrence of occasional bursts and pulsations near the nozzle exit producing very small gas bubbles circulating around the jet. The frequency of these bursts was of the order of a few per second and depended somewhat on the flow rate. An example of the jet behavior is shown in Fig. 3, which is a single-frame stroboscopic picture for a plenum air pressure of 30 psig. As shown, the jet emerged from the nozzle in a continuous cone having a diffusion angle of 23 degrees. This behavior had been previously observed by Bell, Boyce and Collier [7].

Plume Length Data

Two series of runs involving the injection of HCl gas into aqueous solutions of NH_3 were made, one at a plenum stagnation pressure, P_s, of 20 psig (0.239 MPa) and another at P_s = 40 psig (0.377 MPa). Both plenum pressures were more than sufficient to cause flow choking at the injector nozzle. The mass fraction of ammonia in the solution, $Y_{F\infty}$, ranged from 0.024 to 0.30. All runs were made at room temperature, using a 1-mm diameter injector nozzle. For each run, a single-frame stroboscopic picture was taken of the penetration of the gaseous jet into the ammonia solution ("plume"). The plume length was determined from analysis of the stroboscopic picture taken. For each experimental condition, four identical runs were made. (One

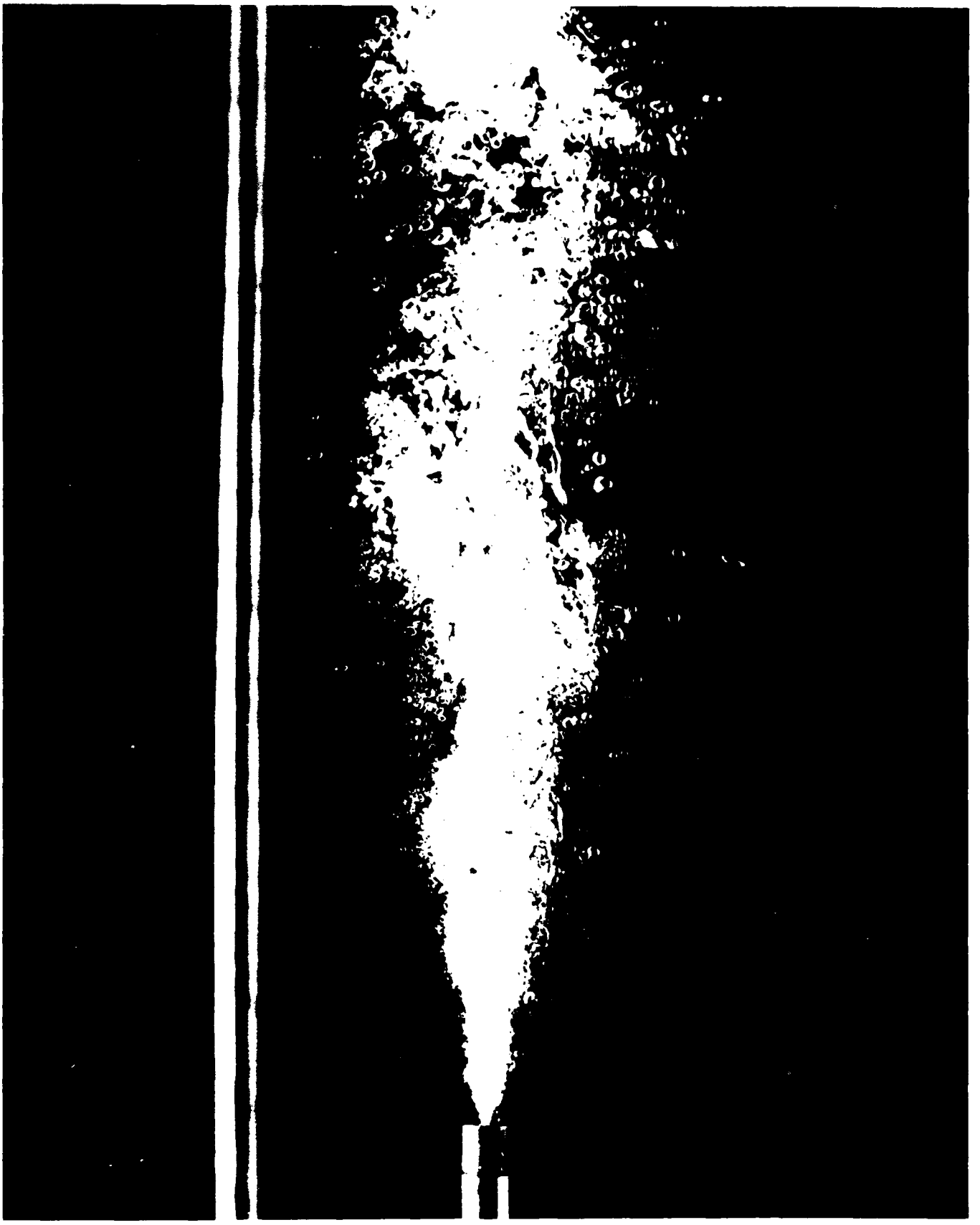

Fig. 3. Sonic Jet of Air Submerged in Water

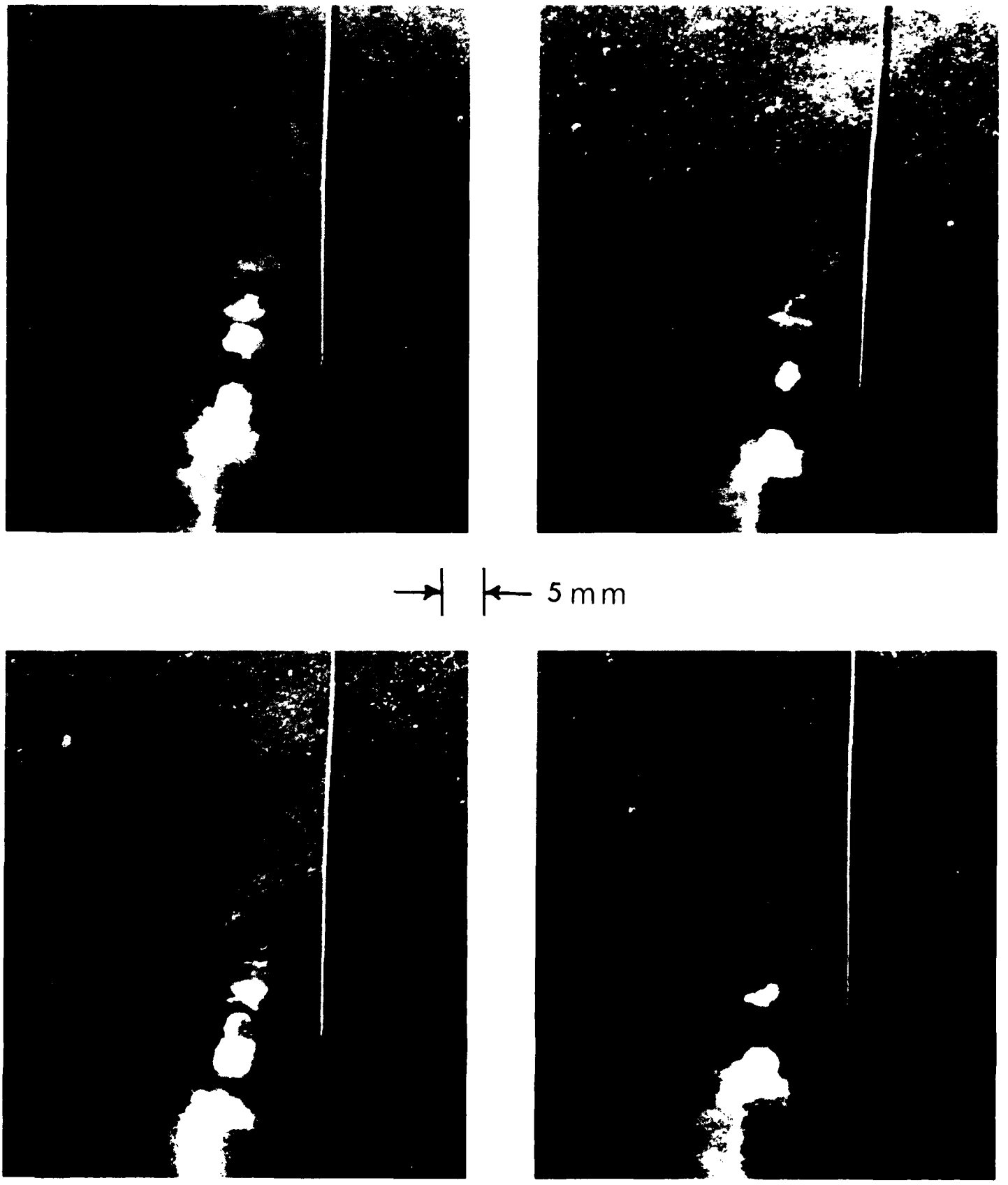

Fig. 4. Stroboscopic Pictures of Reacting Plumes

exception was for the case of P_s = 20 psig and $Y_{F\infty}$ = 0.024 where only two identical runs were made.) The four pictures shown in Fig. 4 correspond to the four runs made for the case of P_s = 40 psig and $Y_{F\infty}$ = 0.105.

The results for P_s = 20 psig are presented in Fig. 5 and those for P_s = 40 psig in Fig. 6. The plume length divided by the injector diameter, L/d_o, is plotted as a function of the ammonia concentration, $Y_{F\infty}$. All data points are denoted by circles with a line drawn through four identical runs for each experimental condition. It is seen that the scatter in the data is very large. This scatter is not surprising in view of the high-speed motion picture studies which will be described in the next section. The high-speed motion pictures taken show that the shape of the plume is not stationary, but undergoes a periodic change and that the plume length varies over a wide range during a time period of about 1 msec. The plume lengths measured here represent those values which were seen by the camera during any 200-μsec interval of the period. Also, the data reported here refer to those plume lengths attached to the injector nozzle and do not include detached bubbles which are discussed in the next section. (These detached bubbles are also seen in Fig. 4.)

Despite the large amount of scatter, it is seen that the plume length increases with increasing concentration of ammonia for large values of $Y_{F\infty}$ (say, greater than 0.15). For small values of $Y_{F\infty}$, it appears that the plume length remains fairly constant. Also shown in Figs. 5 and 6 for comparison are three curves based on Eqs. (A3), (A15) and (A16) discussed in the Appendix. These curves were calculated using the following assumed values of constants: C_1 = 5.68 (value consistent with the correlation of Avery and Faeth [5]), C_2 = 0.32 (entrainment coefficient of Ricou and Spalding [11]), C_3 = 1.0, $C_4 = C_1$, and ΔH_{rea} = 818 cal/gHCl.

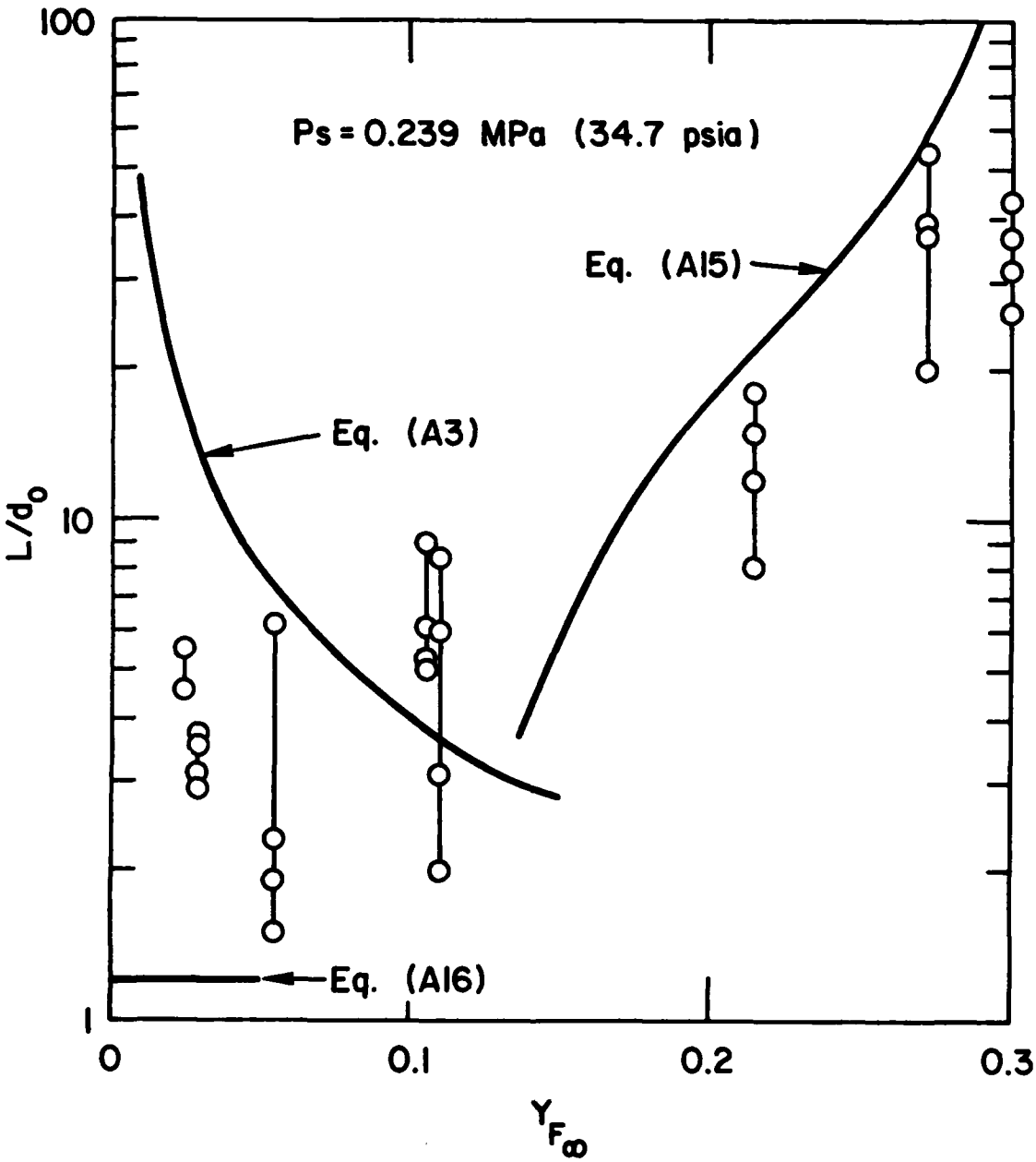

Fig. 5. Plume Length Data for HCl Plenum Stagnation Pressure of 20 psig (0.239 MPa)

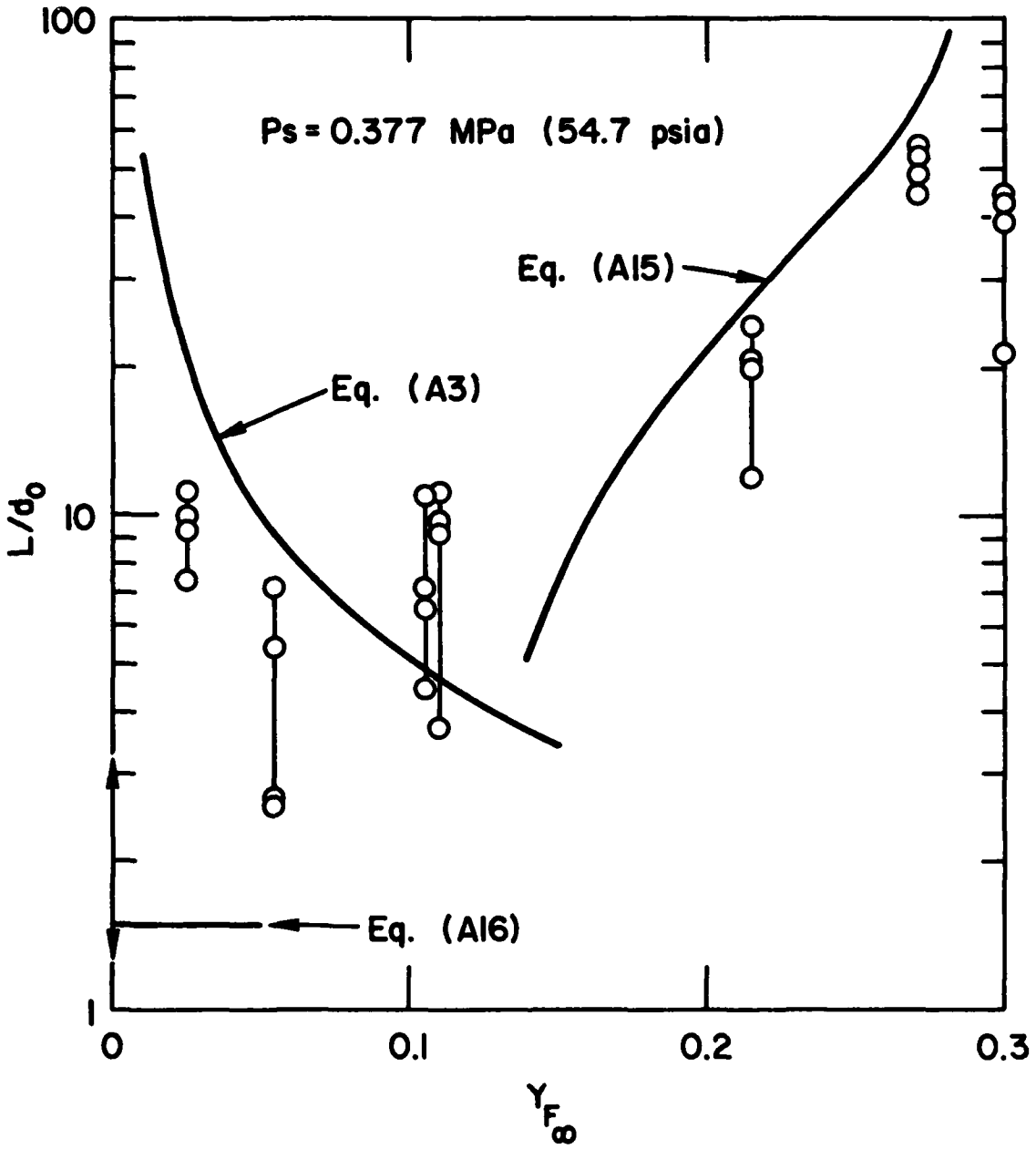

Fig. 6. Plume Length Data for HCl Plenum Stagnation Pressure of 40 psig (0.377 MPa)

Discussion

The trends in the data for large values of $Y_{F\infty}$ appear to be consistent with the prediction based on Eq. (A15); namely, the plume length increases with increasing concentration of ammonia. As discussed in the Appendix, this effect of ammonia concentration on the plume length arises due to the excess ammonia vapor produced by the heat of reaction. When the amount of ammonia vaporization is large, the plume length is mostly determined by the distance required for condensation of the vaporized ammonia. The boiling point of an aqueous solution of ammonia (hence, the degree of subcooling for a given solution temperature) decreases with increasing concentration of ammonia. Given the heat of reaction, therefore, the amount of ammonia vaporization increases with increasing concentration. Thus, the higher the ammonia concentration, the larger the plume length. In contrast, Eq. (A3), which ignores the vaporization of ammonia, would predict a plume length decreasing with increasing concentration of ammonia.

The plume lengths for small values of $Y_{F\infty}$, while remaining fairly constant, appear to be significantly greater than those which might be expected for the case of pure dissolution. A range of plume lengths for the dissolution of HCl gas in pure water at P_s = 40 psig is indicated by arrows in Fig. 6. This data, which was obtained from a high-speed motion picture taken of a dissolving jet, appears to be in fair agreement with the prediction given by Eq. (A16). As indicated in the Appendix, if the reaction occurs in the liquid solution phase with negligible vaporization of ammonia, the plume length would largely be determined by the dissolution process. In fact, the plume length should not exceed that for pure dissolution. The fact that this is not the case seems to suggest that the vaporization of ammonia may take place and play a role even for small concentrations of ammonia. For small concentrations of

ammonia, most of the injected HCl gas is likely to be dissolved in the liquid solution, reacting with ammonia there. Depending on the local mixing condition, the combined heat of dissolution and reaction would be sufficient to cause some vaporization of the solution. (The heat of dissolution alone could raise the solution temperature to the boiling point.)

The vaporization could influence the plume length in various ways. If there is any excess ammonia vapor produced, the distance required for condensation of the vapor would add to the plume length. For large concentrations of ammonia, this would be the predominant effect and the plume would consist mostly of ammonia vapor. For small concentrations, the vaporization is not likely to be as extensive, so the condensation length of the vapor might not be significant. However, the local vaporization near the injector exit could momentarily impede the entrainment of the ammonia solution into the HCl gas jet, thus allowing the jet to penetrate further into the bath. As a result, the plume length might increase. This hypothesis regarding the effect of vaporization on mixing is further discussed in the next section in connection with the periodic phenomena observed in high-speed motion picture studies.

IV. High-Speed Motion Picture Studies

During the runs made for the plume length data, a high-pitched sound (shriek) was invariably heard. To investigate the nature of the sound, a few selected runs were made in which pressure fluctuations near the injector nozzle were measured. At the same time, high-speed motion pictures of the resulting plumes were also taken. These motion pictures showed that the plumes were not stationary, but underwent a change in shape and size with time, which appeared to be periodic or cyclic. The pressure measurements also exhibited similar periodic fluctuations, which undoubtedly were responsible

for the high-pitched sound heard. It soon became obvious that the pressure fluctuations were closely related to the periodic behavior of the plumes. Following this initial discovery of the periodic nature of the plume behavior, extensive high-speed motion picture studies along with pressure fluctuation measurements were undertaken covering a wide range of ammonia concentrations at the plenum stagnation pressure of 40 psig. (Initial scoping studies indicated that the plume behavior at P_s = 20 psig differed little from that at 40 psig.) The salient features of the results of these studies are summarized below. Unless otherwise noted, all runs were made at room temperature.

Periodic Plume Behavior

The plume behavior, although qualitatively similar, exhibited a varying degree of regularities depending on the ammonia concentration. We shall focus on the case of $Y_{F\infty} \cong 0.1$, where the observed periodic behavior of the plume was most distinct as well as reproducible. This case will be called the "reference" case.

Figure 7 shows selected frames from a high-speed motion picture taken of the injection of HCl gas into a pool of 6-Normal aqueous solution of NH_3 (the corresponding mass fraction of NH_3 in the solution was 0.11). The HCl gas plenum pressure was 40 psig. This pressure is about two times that needed for flow choking at the nozzle at atmospheric pressure. The pressure at the choking plane was calculated to be 29 psia, so the HCl gas jet when it came out of the nozzle, was underexpanded.

The first frame of Fig. 7 shows the HCl gas jet just about to emerge from the 1-mm diameter nozzle. Also shown is a detached bubble downstream of the nozzle, which has previously been formed due to a breakoff of the plume near the nozzle. The second and third frames show a fairly uniform expansion (axial as well as radial) of the jet occurring at the nozzle exit while the

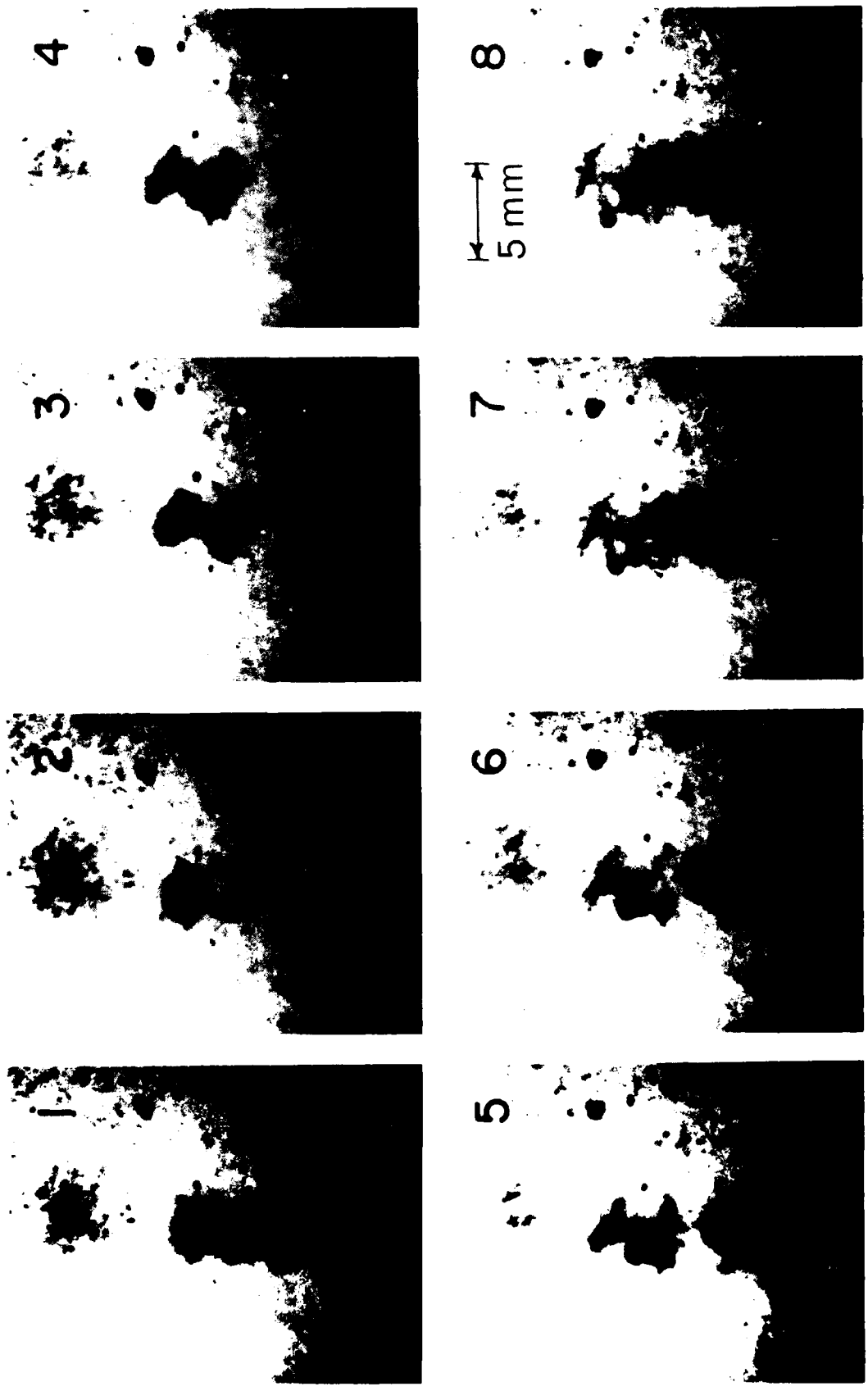

Fig. 7. Selected Frames from a High-Speed Motion Picture of Reacting Plumes ($Y_{F\infty}$ = 0.11 and room temperature)

detached bubble is collapsing. In the fourth frame, the jet begins a predominantly axial expansion. In the fifth and sixth frames the axial expansion of the plume continues while it starts shrinking near the nozzle exit. The necking-down of the plume near the nozzle exit is clearly visible in the seventh frame. The last frame shows the plume breaking off where the necking occurred, producing a detached bubble downstream of the nozzle. This last frame is essentially the same as the first frame, indicating that the process repeats itself. The time interval between two adjacent frames was 0.13 msec and the whole process described above took place in a period of 0.9 msec.

The pressure fluctuations near the nozzle were recorded on an oscilloscope as well as superimposed on the motion picture. A frame-by-frame comparison of the motion picture with the pressure record seems to suggest that the occurrence of the pressure peak probably coincides with the breakoff of the plume from the nozzle. Figure 8 shows an oscilloscope trace for a run made under conditions nearly identical to those for Fig. 7. (The mass fraction of ammonia was 0.12, which was slightly higher than that for Fig. 7, 0.11.) It is seen that the pressure fluctuations were occurring in a remarkably regular manner. Clearly, these well-defined pressure fluctuations were responsible for the high-pitched tone that was heard during the experiment. Figure 9 shows the normalized power spectrum of the pressure fluctuations as a function of frequency. It indicates that the dominant frequency was about 1 kHz, corresponding to a period of 1 msec.

For lower concentrations of ammonia ($Y_{F\infty}$ = 0.025 and 0.055), the overall plume behavior appeared similar to that for the reference case with a somewhat shorter period (say, 0.7 ms as compared to 0.9 ms). However, the individual stages involved were not as distinct as those observed for the reference case.

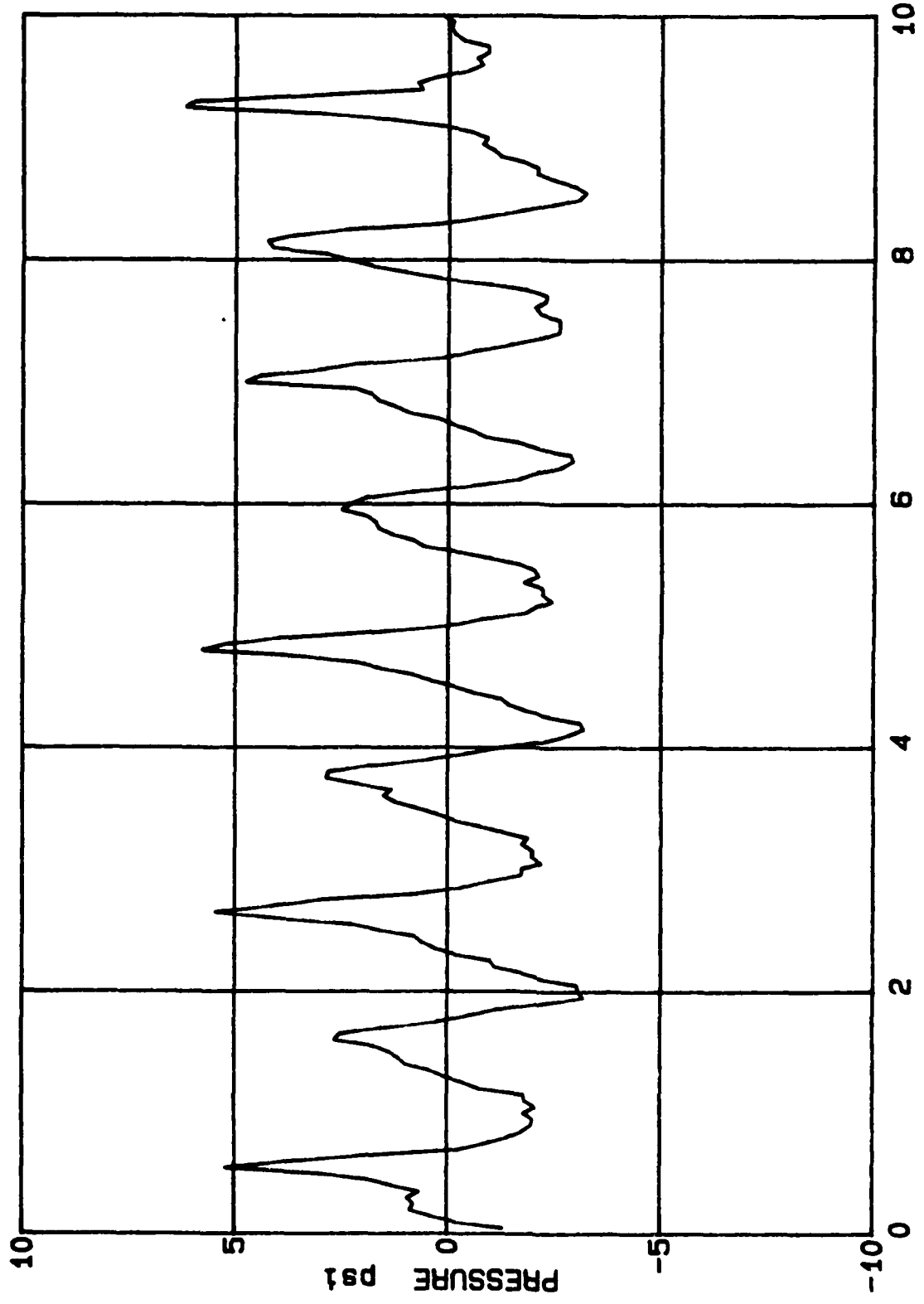

Fig. 8. Oscilloscope Trace of Pressure Fluctuations (Y_{F_∞} = 0.12 and room temperature)

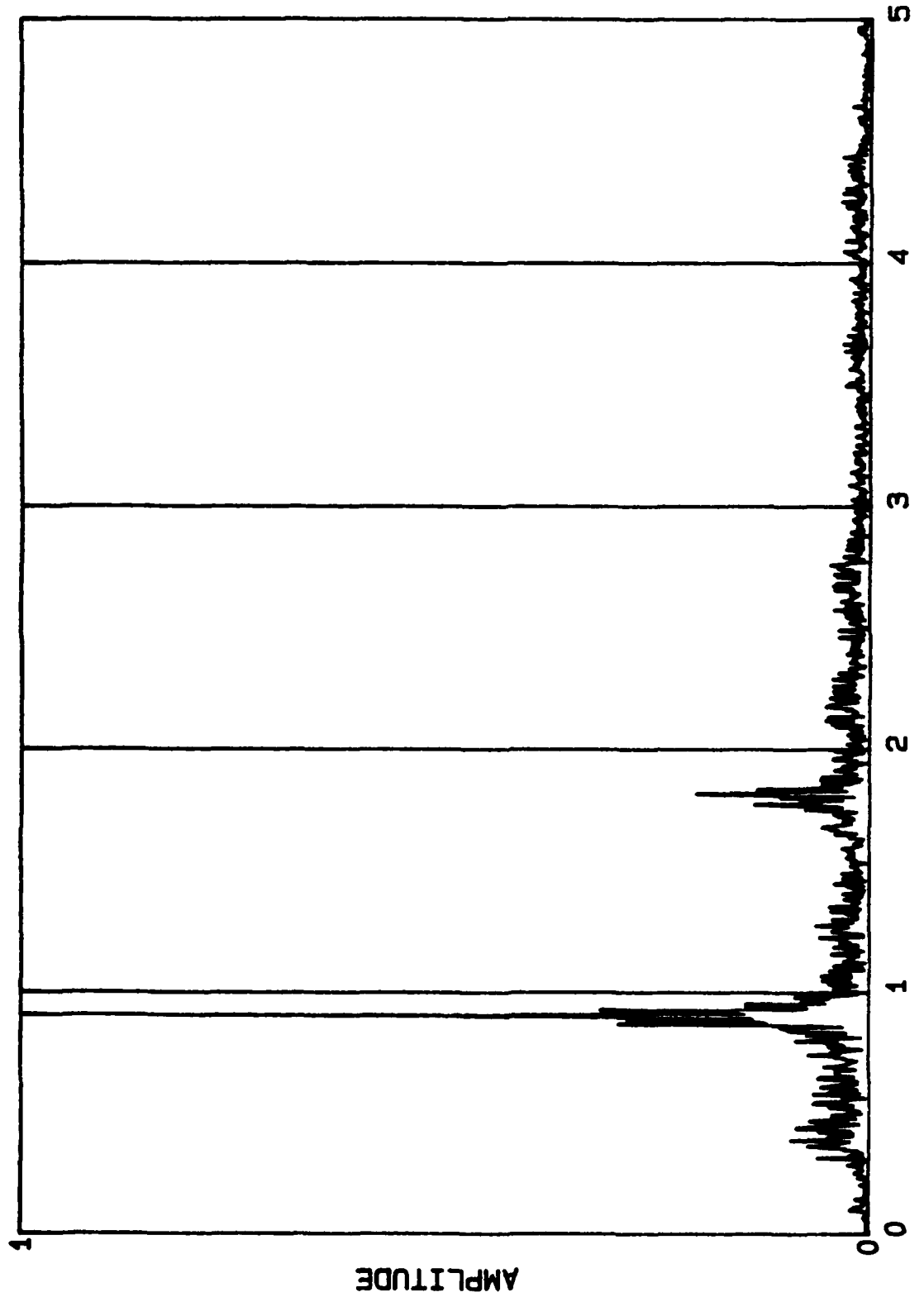

Fig. 9. Normalized Power Spectrum of Pressure Fluctuations ($Y_{F\infty}$ = 0.12 and room temperature)

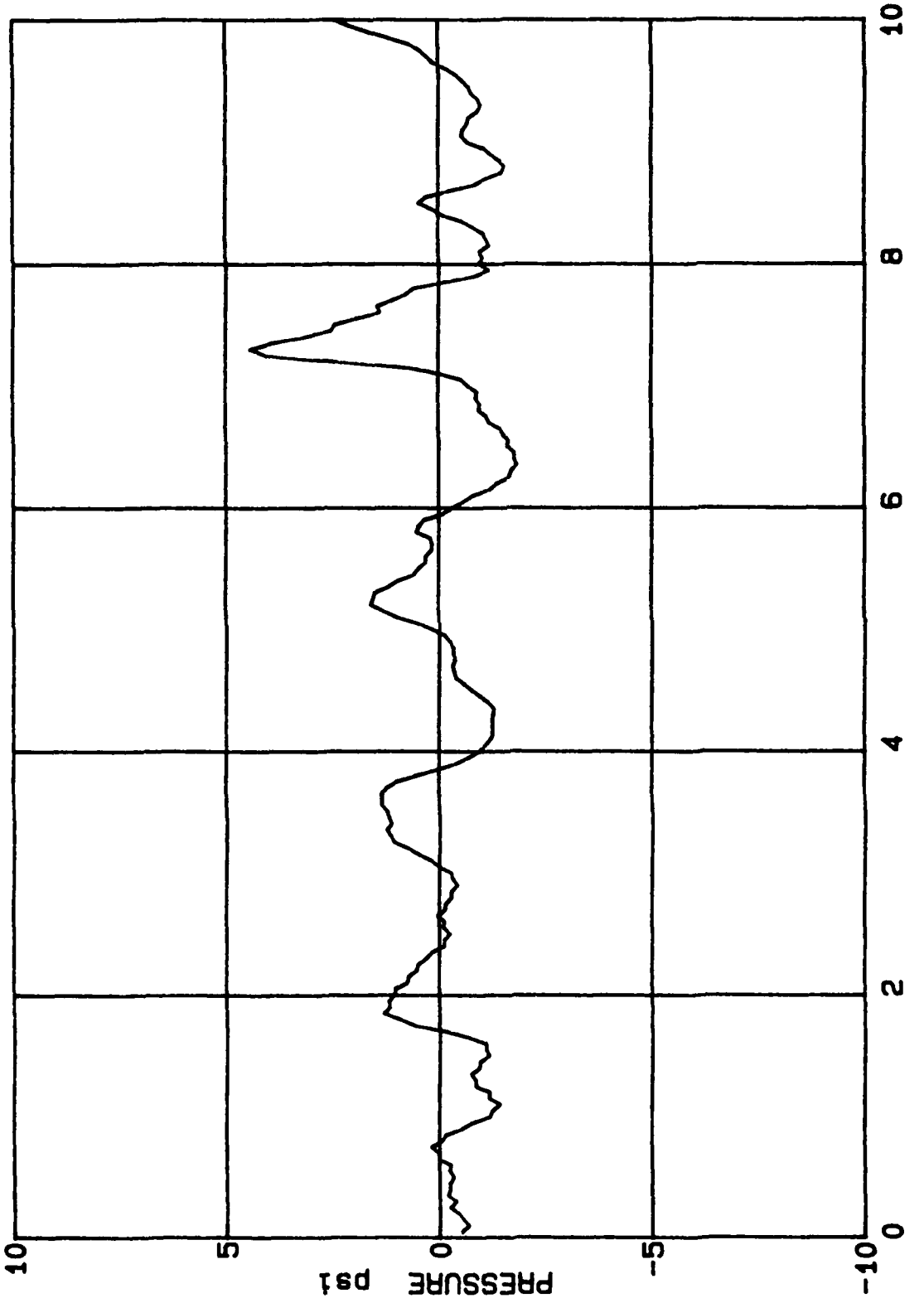

Fig. 10. Oscilloscope Trace of Pressure Fluctuations (Y_{F_∞} = 0.19 and room temperature)

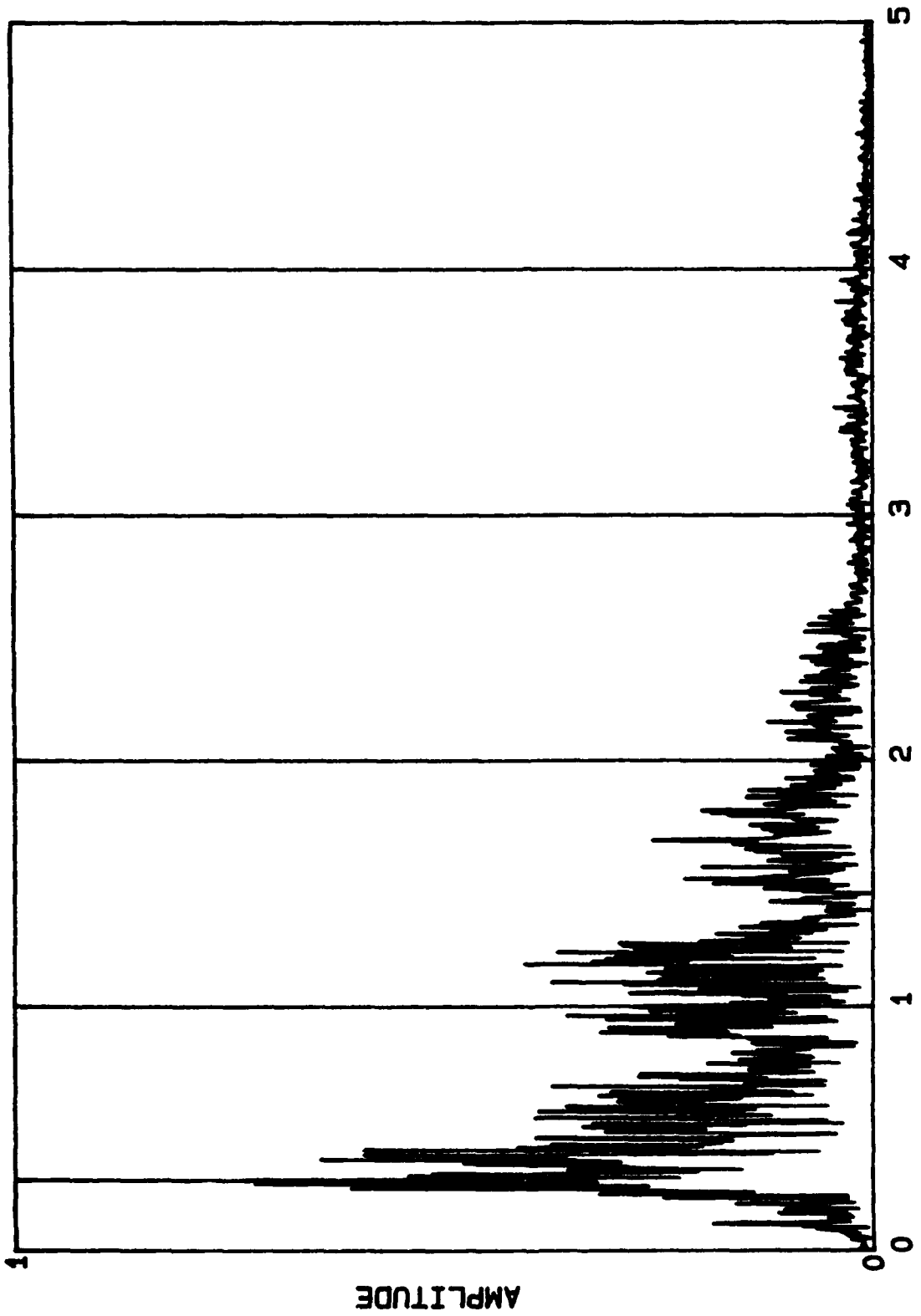

Fig. 11. Normalized Power Spectrum of Pressure Fluctuations (Y_{F_∞} = 0.19 and room temperature)

For higher concentrations of ammonia ($Y_{F\infty}$ = 0.19 and 0.24), it was difficult to discern well-defined periodicity, since variations in the plume shape and size were not quite repetitious. Also, the plume shape and size varied to a much greater extent than it did for the reference case and the breakoff of plume bubbles occurred many nozzle diameters downstream of the nozzle exit. Nevertheless, the overall plume behavior was unmistakably that of cyclic growth and collapse and the period appeared to be in the range of 3 to 5 ms, which is much longer than that for the reference case. Figure 10 shows an oscilloscope trace of the pressure fluctuations for the case of $Y_{F\infty}$ = 0.19. The power spectrum of the pressure fluctuations is shown in Fig. 11 as a function of frequency.

Discussion

The periodic or cyclic plume behavior described above was totally unexpected from the knowledge of the behavior of a condensing jet. Experiments on condensing jets invariably showed that when the vapor flow was sonic, a stable cone of condensing vapor formed at the nozzle exit [8]. Thus, the periodic phenomena observed in the present experiments are considered to be unique to reacting jets. More specifically, it is believed that the periodic phenomena is driven by vaporization of ammonia due to the heat of reaction. The plume growth and collapse is probably related to the formation and condensation (redissolution) of the ammonia vapor in the solution. In an effort to check this hypothesis, an experiment was conducted in which the HCl gas was injected into pure water at room temperature. Although the dissolution of HCl gas in water is accompanied by heat release, calculations indicate that the vaporization of water in this experiment would be unlikely. No periodic or cyclic phenomena was observed in the experiment. A selected movie frame of the dissolving HCl gas jet is shown in Fig. 12. The cone-shaped plume was stable except for very

Fig. 12. Dissolving Jet of HCl in Water

occasional lateral oscillations. Clearly, the behavior of the dissolving HCl gas jet was very similar to that of a condensing vapor jet.

Another experiment was conducted to check the vaporization hypothesis. This experiment was essentially identical to the reference case except for the solution temperature raised to 45°C from room temperature. The high-speed motion picture taken showed that the plume behavior in this experiment was very similar to that for the case of $Y_{F\infty} = 0.19$ and room temperature. Thus, increasing the solution temperature has a similar effect on the plume behavior as does increasing the ammonia concentration. The degree of subcooling (boiling point minus solution temperature) was about the same for this experiment ($Y_{F\infty} = 0.12$ and 45°C) and for the case of $Y_{F\infty} = 0.19$ and room temperature. In as much as the degree of subcooling controls the processes of vaporization and condensation, this experiment lends support to the hypothesis that the observed plume behavior is caused by the vaporization of ammonia from the solution.

As discussed above, the vaporization of ammonia due to the heat of reaction is believed to be responsible for the observed periodic plume behavior. However, no satisfactory explanation has yet been found for the individual stages involved. A plausible sequence of events is as follows. The vaporization of ammonia would cause a local expansion of the plume, which would momentarily impede the entrainment of the ammonia solution into the plume containing the HCl gas. As a result, the plume would stretch out. Once the expansion stops, however, the entrainment mixing would again increase, leading to an increase in reaction and local shrinking of the plume. The plume could locally collapse and break off, forming a detached bubble. The mixing and reaction would be greatly enhanced where the shrinking and collapse takes place. The reaction heat released then would cause local vaporization of

ammonia and the whole process would repeat itself. This postulated sequence of events is based on an inspection of the selected movie frames shown in Fig. 7. At the moment, it is more of a speculation than an explanation.

V. Concluding Remarks

The results of the present study indicate that the behavior of a reacting gas jet submerged in a liquid is highly dynamic and complex, depending on the extent of vaporization of the bath liquid caused by reaction heat release. The vaporization would influence the length of the gaseous jet penetration ("plume") in two ways. First, the distance required for condensation of any excess vapor would add to the plume length. Second, the vaporization might interfere with the entrainment of the bath liquid into the reacting plume, thereby influencing the extent of mixing and reaction.

The periodic plume behavior observed in the present experiment is extremely interesting and requires a further study. In particular, the observations made for the reference case, including a high-pitched sound, exhibit a striking similarity to the so-called "singing flame" phenomenon that has been known for a long time [9,10]. As in the singing flame, the remarkably distinct periodic phenomena observed may be related to resonance between the oscillation of the reacting plume and that of the surrounding medium, which in the present experiment, would be the pool of ammonia solution.

It remains to be seen whether periodic phenomena similar to those observed in the present NH_3/HCl system will also occur in other reacting systems including liquid metals. However, it would be important to remember the dynamic nature of the plume behavior when using an X-ray imaging technique for visualization of a reacting gas jet in a liquid metal bath. As compared to visual-light photography, X-ray imaging has numerous limitations in terms

of time resolution and contrast, so it may be difficult to discern a dynamic event occurring over a short period of time (say, 1 msec or less).

While the observations made in the present study are of a preliminary nature, they may have important scientific and practical implications. In particular, it appears that the near-field mixing of the injected gas and the bath liquid is greatly affected by the vaporization of the bath liquid due to reaction heat release. The near-field mixing and reaction is an important consideration in understanding the erosion behavior of the injector nozzle. Also, the vaporization might have a significant effect on the circulation pattern of the bath liquid. To understand these implications better, a refined experiment including detailed measurements of temperature, concentration and void fraction distributions would be necessary.

References

1. Biermann, U. K. P. (1975), "The Lithium/Sulphurhexafluoride Heat Source in Combination with a Stirling Engine as an Environmental Independent Underwater Propulsion System," Proceedings of Tenth Intersociety Energy Conference, pp. 1023-1030.

2. van der Sluys, W. L. N. (1975), "A Lithium/Sodium/Sulphurhexafluoride Heat Source in Combination with a Stirling Engine as a Propulsion System for Small Submersibles," ibid., pp. 1031-1037.

3. Groff, E. G. and Faeth, G. M. (1978), "A Steady Metal Combustor as a Closed Thermal Energy Source," Journal of Hydronautics, 12, pp. 63-70.

4. Mattavi, J. N., Heffner, F. E., and Miklos, A. A. (1969), "The Stirling Engine for Underwater Vehicle Applications," SAE Transactions, Vol. 78, Sect. 4, pp. 2376-2400.

5. Avery, J. F. and Faeth, G. M. (1975), "Combustion of a Submerged Gaseous Oxidizer Jet in a Liquid Metal," Fifteenth Symposium (International) on Combustion, The Combustion Institute, Pittsburgh, pp. 501-512.

6. Chen, L. D. and Faeth, G. M. (1983), "Structure of Turbulent Reacting Gas Jets Submerged in Liquid Metals," Combustion Science and Technology, 11, pp. 111-131.

7. Bell, R., Boyce, B. E., and Collier, J. G. (1972), "The Structure of a Submerged Impinging Gas Jet," J. Brit. Nucl. Energy Soc., 11, pp. 183-193.

8. Cumo, M., Farello, G. E., and Ferrari, G. (1978), "Direct Heat Transfer in Pressure-Suppression Systems," Sixth International Heat Transfer Conference, Vol. 5, Toronto, Canada, pp. 101-106.

9. Lord Rayleigh (1945), The Theory of Sound, New York, Dover, pp. 227-230.

10. Richardson, E. G. (1923), "The Theory of the Singing Flame," Proc. Phys. Soc. London, 35, pp. 47-54.

11. Ricou, F. P. and Spalding, D. B. (1961), "Measurements of Entrainment by Axisymmetrical Turbulent Jets," J. Fluid Mech., 11, pp. 21-32.

12. Hill, B. J. (1972), "Measurement of Local Entrainment Rate in the Initial Region of Axisymmetric Turbulent Air Jets," ibid., 51, pp. 773-779.

13. Carreau, J. L., Loukarfi, L., Gbahoue, L., Hobbes, P., and Roger, F. (1985), "Hydrodynamics of an Axisymmetric, Submerged Non-reactive Gas Jet -- Measurement of Entrainment -- Contribution to the Wastage Modeling," Proceedings of the 19th IECEC, Paper No. 859176, pp. 1.688-1.693.

14. Perry, J. H., Ed. (1950), Chemical Engineers Handbook, Third Edition, McGraw-Hill, New York.

Appendix: Plume Length Correlations

When a reacting gas jet is injected into a liquid bath, the jet penetrates only a finite distance into the bath because the gas is consumed by reactions in the bath. The reaction can be condensation in a subcooled liquid, dissolution in an unsaturated liquid, or chemical reaction with a reactant dissolved in the liquid. The penetration of the gaseous jet into the liquid bath is often referred to as "plume". In this Appendix we shall use a simple concept of entrainment and mixing to derive correlations for the plume length for three cases, namely chemical reaction with no fuel vaporization, chemical reaction with fuel vaporization, and simple dissolution. These correlations have been used for comparison with experimental data in Section III.

Reacting jets with no fuel vaporization

Consider a pure oxidizer gas jet discharging into a bath of liquid fuel. The oxidizer gas is consumed by reacting with the fuel entrained from the liquid bath. The plume length L is equal to the reaction zone length L_r. We assume that the mixing ratio of the fuel and oxidizer in the reaction zone over length L_r is proportional to the stoichiometric ratio, viz.,

$$\frac{Y_{F\infty}\dot{m}_{\infty}(L_r)}{\dot{m}_o} = C_1\,\phi \qquad \text{(A1)}$$

where $Y_{F\infty}$ is the mass fraction of fuel in the bath liquid, $\dot{m}_{\infty}(L_r)$ is the rate of entrainment of the bath fluid into the gas jet over length L_r, $\dot{m}_o$ is the oxidizer gas flow rate at the injector nozzle, ϕ is the stoichiometric fuel-to-oxidizer mass ratio, and C_1 is a constant greater than unity which allows

for imperfect mixing and is to be determined empirically. For a turbulent jet discharging into a large reservoir of fluid at rest, it has been experimentally established [11,12] that the entrainment rate $\dot{m}_\infty$ is related to the nozzle flow rate $\dot{m}_o$ by

$$\frac{\dot{m}_\infty(L_r)}{\dot{m}_o} = C_2 \left(\frac{L_r}{d_o}\right)\left(\frac{\rho_\infty}{\rho_o}\right)^{1/2} \tag{A2}$$

where d_o is the nozzle diameter, ρ_∞ and ρ_o are the densities of the bath liquid and the oxidizer gas at the nozzle exit, respectively, and C_2 is an empirical constant. Combining Eqs. (A1) and (A2), we have

$$\frac{L_r}{d_o} = \frac{C_1}{C_2}\frac{\phi}{Y_{F\infty}}\left(\frac{\rho_o}{\rho_\infty}\right)^{1/2} \tag{A3}$$

Avery and Faeth [5] found that with $C_1/C_2 = 17.8$, Eq. (A3) agreed reasonably well with a number of condensing and reacting jet data. If we use $C_2 = 0.32$, the value obtained by Ricou and Spalding [11], we find that $C_1 = 5.68$. This implies that the amount of fuel mixed with the oxidizer in the reaction zone is 5 to 6 times larger than the stoichiometric requirement.

The entrainment law given by Eq. (A2) was originally established for a subsonic gas jet in air. For an underexpanded sonic jet where the jet exit pressure is greater than the ambient pressure, the pressure difference between the jet exit plane and the ambient atmosphere gives rise to an excess momentum. This excess momentum is not explicitly taken into account in Eq. (A2). Recently, however, Carreau et al. [13] conducted experiments on liquid entrainment for sonic jets of nitrogen gas in water and found that Eq. (A2) was valid with a C_2 value of 0.30, which is surprisingly close to the entrainment coefficient of Ricou and Spalding [11]. Thus it appears reasonable to use Eq. (A2) as an empirical law even for underexpanded sonic jets.

Reacting jets with fuel vaporization

If the entrained liquid fuel vaporizes due to the heat of reaction, the overall jet penetration length could be larger than the reaction zone length, i.e. the "plume" could be longer than the "flame." The overall penetration length (L) may be estimated by adding the reaction zone length (L_r) and the length required for condensation of fuel vapor (L_c), viz.

$$L = L_r + L_c \tag{A4}$$

We now estimate the condensation length, L_c, for the case of an oxidizer jet submerged in a bath of pure fuel liquid ($Y_{F\infty} = 1.0$), such as the injection of chlorine gas into sodium liquid.

Let $\dot{Q}_r$ be the rate of reaction heat release available for heating and vaporizing the entrained fuel. If the mass rate of fuel addition to the vaporizing zone is $(\dot{m}_\infty)_{vap}$, an energy balance gives

$$\dot{Q}_r = (\dot{m}_\infty)_{vap} \left(C_p \, \Delta T + X_{vap} \, \Delta H_{vap}\right) \tag{A5}$$

where C_p is the specific heat of the fuel liquid, $\Delta T = T_{sat} - T_\infty$ is the degree of subcooling of the reservoir fuel liquid, X_{vap} is the vapor quality and ΔH_{vap} is the heat of vaporization. Now, we assume that $(\dot{m}_\infty)_{vap}$ is proportional to the rate of fuel entrainment into the reaction zone, $(\dot{m}_\infty)_r = \dot{m}_\infty (L_r)$, viz.

$$(\dot{m}_\infty)_{vap} = C_3 \, (\dot{m}_\infty)_r \tag{A6}$$

where C_3 is expected to be of the order of unity. Further, we have

$$\dot{Q}_r = \dot{m}_o \, \Delta H_{rea} \tag{A7}$$

where ΔH_{rea} is the heat of reaction at prevailing condition whose exact value depends, among others, on the enthalpy of the product species. Substitution of Eqs. (A6) and (A7) into Eq. (A5) gives

$$\dot{m}_o \, \Delta H_{rea} = C_3 \, (\dot{m}_\infty)_r \, (C_p \, \Delta T + X_{vap} \, \Delta H_{vap}) \tag{A8}$$

If the vapor quality, X_{vap}, is zero or negative, no vaporization of fuel occurs and the condensation length, L_c, would be zero. The enthalpy flow associated with the fuel vapor is

$$C_3 \, (\dot{m}_\infty)_r \, X_{vap} \, \Delta H_{vap} = \dot{m}_0 \, \Delta H_{rea} - C_3 \, (\dot{m}_\infty)_r \, C_p \, \Delta T \tag{A9}$$

We now assume that this enthalpy flow of fuel vapor is quenched by the cold reservoir fuel liquid entrained over the condensation length, L_c. A simple energy balance over L_c gives

$$(\dot{m}_\infty)_c \, C_p \, \Delta T = C_4 \, C_3 \, (\dot{m}_\infty)_r \, X_{vap} \, \Delta H_{vap} \tag{A10}$$

where $(\dot{m}_\infty)_c = \dot{m}_\infty(L_c)$ is the entrainment rate of the bath liquid over the condensation length, L_c, and C_4 is a proportional constant which is expected to be of the same order of magnitude as C_1. $(\dot{m}_\infty)_c$ may be obtained from an entrainment law, such as used to derive the reaction zone length, viz.

$$\frac{(\dot{m}_\infty)_c}{\dot{m}_o} = C_2 \, \left(\frac{L_c}{d_o}\right)\left(\frac{\rho_\infty}{\rho_o}\right)^{1/2} \tag{A11}$$

Combination of Eqs. (A9), (A10) and (A11) and rearrangement yields

$$\frac{L_c}{d_o} = \frac{C_4}{C_2}\left(\frac{\rho_o}{\rho_\infty}\right)^{1/2}\left[\frac{\Delta H_{rea}}{C_p \Delta T} - C_3 \frac{(\dot{m}_\infty)_r}{\dot{m}_o}\right]$$

$$= \frac{C_4}{C_2}\left(\frac{\rho_o}{\rho_\infty}\right)^{1/2}\left[\frac{\Delta H_{rea}}{C_p \Delta T} - C_3 C_1 \phi\right] \qquad \text{(A12)}$$

Combination of Eqs. (A3) and (A12) gives the overall plume length, L,

$$\frac{L}{d_o} = \frac{L_r + L_c}{d_o} = \frac{1}{C_2}\left(\frac{\rho_o}{\rho_\infty}\right)^{1/2}\left[C_1 (1 - C_3 C_4)\phi + C_4 \frac{\Delta H_{rea}}{C_p \Delta T}\right] \qquad \text{(A13)}$$

Strictly, the preceding derivation only applies to the case of a pure fuel bath. For the NH_3/HCl system, which was used in the present experiment, the treatment of fuel vaporization would be very complicated, since it involves two-component boiling, i.e. distillation. The boiling point of an NH_3 aqueous solution depends on the concentration of NH_3. Given the initial NH_3 concentration, $Y_{F\infty}$, and temperature, T_∞, Eq. (A8) may be used along with a boiling curve diagram* in order to determine whether or not there would be any vaporization at all. For the case when the NH_3 solution vaporizes, equilibrium distillation may be assumed to determine the vapor quality, X_{vap}. Generally, the determination of X_{vap} is numerically tedious as it involves simultaneous consideration of the liquid-vapor composition and enthalpy-concentration diagrams. Similar complications would arise in calculating the condensation process. For our present purposes, we shall only consider the

*Information necessary to construct a boiling curve diagram for aqueous solutions of NH_3 may be found in the chemical engineering literature. See, for example, Ref. [14].

case when $X_{vap} << 1$. In this case, all the equations derived for the pure fuel case are approximately valid with Eqs. (A12) and (A13) modified as follows.

$$\frac{L_c}{d_o} = \frac{C_4}{C_2} \left(\frac{\rho_o}{\rho_\infty}\right)^{1/2} \left[\left(\frac{\Delta H_{rea}}{C_p \Delta T}\right) - C_3 C_1 \left(\frac{\phi}{Y_{F\infty}}\right)\right] \tag{A14}$$

and

$$\frac{L}{d_o} = \frac{1}{C_2} \left(\frac{\rho_o}{\rho_\infty}\right)^{1/2} \left[C_1 (1 - C_3 C_4) \left(\frac{\phi}{Y_{F\infty}}\right) + C_4 \left(\frac{\Delta H_{rea}}{C_p \Delta T}\right)\right] \tag{A15}$$

Dissolving jets

For the injection of HCl gas into an aqueous solution of NH_3, the injected HCl gas would disappear even when the NH_3 concentration is zero, because of dissolution of the HCl gas in the water. If the reaction between NH_3 and HCl is solely gas-phase, much dissolution of HCl gas in the water is unlikely and the disappearance of HCl gas due to dissolution may be unimportant. If the reaction occurs mainly in the liquid phase (i.e. aqueous solutions of NH_3), the plume length, in the absence of fuel vaporization, would largely be determined by the dissolution process.

For dissolving jets of HCl gas in pure water, the plume length may be estimated based on the same approach as used for the reaction zone length. It can be shown that the plume length due to dissolution, L_d, is given by

$$\frac{L_d}{d_o} = \frac{C_1}{C_2} \left(\frac{1 - Y^*_{HCl}}{Y^*_{HCl}}\right)\left(\frac{\rho_o}{\rho_\infty}\right)^{1/2} \tag{A16}$$

where Y^*_{HCl} is the mass fraction of HCl corresponding to the solubility limit in the water bath and C_1 and C_2 are the empirical constants discussed earlier.

The dissolution of HCl gas in water is accompanied by liberation of heat. Therefore, if the initial water temperature is sufficiently high, some of the entrained water in the dissolving jet might vaporize. Should this happen, the plume length would be larger than the dissolution length, L_d, given by Eq. (A16). Even if there is no vaporization, the heat of dissolution would raise the temperature of the entrained water to a value higher than the bath temperature. Since the solubility of HCl gas decreases with increasing water temperature, Eq. (A16) would somewhat underestimate the dissolution length when the solubility limit at the bath temperature is used.

Distribution for ANL-86-41

Internal:

C. E. Till
J. F. Marchaterre
L. W. Deitrich
A. J. Goldman
D. Rose
B. W. Spencer
D. R. Pedersen
D. R. Armstrong
R. P. Anderson
L. Bova
D. W. Condiff
J. G. Daley
M. Ishii
J. M. Kramer
D. H. Cho (25)
ANL Patent Dept.
ANL Contract File
ANL Libraries
TIS Files (3)

External:

DOE-TIC (2)
Manager, Chicago Operations Office, DOE
Reactor Analysis and Safety Division Review Committee:
W. B. Behnke, Jr., Commonwealth Edison Co., Chicago, IL 60690
W. P. Chernock, Combustion Engineering, Inc., Windsor, CT 06095
J. M. Hendrie, Brookhaven National Laboratory, Upton, NY 11973
E. A. Mason, Amoco Corp., Naperville, IL 60566
M. J. Ohanian, Univ. of Florida, Gainesville, FL 32611
R. L. Seale, Univ. of Arizona, Tucson, AZ 85721

ONR REPORT DISTRIBUTION LIST
CLOSED, LIQUID METAL COMBUSTION

	One copy except as noted
Dr. Richard S. Miller Mechanics Division Office of Naval Research 800 N. Quincy Street Arlington, VA 22217	2
Defense Documentation Center Building 5, Cameron Station Alexandria, VA 22313	12
Technical Information Division Naval Research Laboratory 4555 Overlook Avenue SW Washington, DC 20375	6
Dr. Robert Nowak Chemistry Division Office of Naval Research 800 N. Quincy Street Arlington, VA 22217	
Dr. Albert D. Wood Technology Programs Office of Naval Research 800 N. Quincy Street Arlington, VA 22217	
Dr. H. W. Carhart Combustion & Fuels Naval Research Laboratory Washington, DC 20375	
Professor Allen Fuhs Department of Aeronautics Naval Post Graduate School Monterey, CA 93943	
Division Director Engineering and Weapons US Naval Academy Annapolis, MD 21402	
Mr. Francis J. Romano Code 63R3 Naval Sea Systems Command Washington, DC 20363	

Mr. Robert Tompkins
Code 36621, Bldg 126T
Naval Underwater Systems Center
Newport, RI 02841

Mr. Maurice F. Murphy
Code R33, Room 4-1711
Naval Surface Weapons, White Oak
Silver Spring, MD 20910

Dr. Kurt Mueller
Code R10
Energetic Materials Division
Naval Surface Weapons Center, White Oak
Silver Spring, MD 20910

Dr. Lynn A. Parnell
Code 634
Naval Ocean Systems Center
San Diego, CA 92152-5000

Dr. Earl Quandt, Jr.
Code 2704
David Taylor Naval Ship
Research and Development Center
Annapolis, MD 21402

Mr. Richard Bloomquist
Code 2752
David Taylor Naval Ship
Research and Development Center
Annapolis, MD 21402

Dr. Lawrence P. Cook
High Temperature Processes Group
National Bureau of Standards
Washington, DC 20234

Professor A. Murty Kanury
Department of Mechanical Engineering
Oregon State University
Corvallis, OR 97331

Professor Irvin Glassman
Department of Mechanical & Aerospace Engineering
Engineering Quadrangle
Princeton University
Princeton, NY 08544

Professor Norman Chigier
Department of Mechanical Engineering
Carnegie-Mellon University
Pittsburgh, PA 15213

Professor George Janz
Cogswell Laboratory, R306
Department of Chemistry
Rensselaer Polytechnic Institute
Troy, NY 12181

Dr. Leonard Leibowitz
Chemical Technology Division
Argonne National Laboratory
9700 South Case Avenue
Argonne, IL 60439

Professor John Tarbell
104 Fenske Laboratory
Pennsylvania State University
University Park, PA 16801

Professor Thomas E. Daubert
104 Fenske Laboratory
Pennsylvania State University
University State Park, PA 16801

Dr. J. Braunstein
Research Division
Oak Ridge Operations
Department E
Oak Ridge, Tennessee 37831

Mr. Norman D. Hubele
MS 1207-4R
Garrett Fluid Systems Company
1300 West Warner Road
Tempe, AZ 85282

Dr. Hugh H. Darsie
Advanced Technology Group
Sunstrand Energy Systems
4747 Harrison Avenue
Rockford, IL 61101

Professor Gerard M. Faeth
Department of Aerospace Engineering
University of Michigan
Ann Arbor, MI 48109

Dr. Dan H. Kiely
Power & Energy Group
The Pennsylvania State University
Applied Research Laboratory
P.O. Box 30
State College, PA 16801

Professor Darryl E. Metzger
Department of Mechanical &
Aerospace Engineering
Arizona State University
Tempe, AZ 85281

Dr. Dae H. Cho
Reactor Analysis & Safety Division
Argonne National Laboratory
Argonne, IL 60439

Professor S. H. Chan
Department of Mechanical Engineering
The University of Wisconsin-Milwaukee
P.O. Box 784
Milwaukee, WI 53201

Professor George A. Brown
Department of Mechanical Engineering
and Applied Mechanics
University of Rhode Island
Kingston, RI 02881

Professor Paul E. Dimotakis
Mail Code 301-46
Graduate Aeronautical Laboratory
California Institute of Technology
Pasadena, CA 91125

Dr. Charles H. Berman
Aerochem Research Laboratories, Inc.
P.O. Box 12
Princeton, NJ 08542

Dr. Donald M. McEligot
Manager, Thermohydromechanics Research
Gould Ocean Systems, Inc.
P.O. Box 4282
Middletown, RI 02840

Dr. C. William Kauffman
Department of Aerospace Engineering
The University of Michigan
Ann Arbor, MI 48109-2140

Professor Lea D. Chen
Department of Mechanical Engineering
The University of Iowa
Iowa City, IA 52242

LCDR Mike Barry
NISC - 4311
Naval Intelligence Support Center
4301 Suitland Road
Washington, DC 20390

Dr. Raafat H. Guirguis
Laboratory for Computational Physics
Code 4040
Naval Research Laboratory
Washington, DC 20375

Professor John Cimbala
157 Hammond Bldg.
Department of Mechanical Engineering
Pennsylvania State University
University Park, PA 16802

END

12-86

DTIC